The fragment coalescence model

W. J. Llope*
T. W. Bonner Nuclear Laboratory, Rice University, Houston, Texas 77251

S. E. Pratt and N. Frazier
*Theory Department, National Superconducting Cyclotron Laboratory
and Department of Physics, Michigan State University, East Lansing, Michigan 48824*

R. Pak, D. Craig, E. E. Gualtieri, S. A. Hannuschke, N. T. B. Stone, A. M. Vander Molen,
G. D. Westfall, and J. Yee
National Superconducting Cyclotron Laboratory and Department of Physics, Michigan State University, East Lansing, Michigan 48824

R. A. Lacey and J. Lauret
Department of Chemistry, State University of New York at Stony Brook, Stony Brook, New York 11794

A. C. Mignerey and D. E. Russ
Department of Chemistry and Biochemistry, University of Maryland, College Park, Maryland 20742
(Received 9 June 1995)

The extraction of source radii from heavy-ion collisions using coalescence models is explored. A new prescription is presented which considers nucleosynthesis via the coalescence of fragments which is, in particular, more appropriate for intermediate-energy collisions than the previous nucleon coalescence prescriptions. This fragment coalescence model provides an avenue for viewing the breakup stage of heavy-ion reactions that yields valuable complimentary information to two-nucleon and two-fragment correlation measurements. This model was applied to recent experimental data on central 55 and 115 MeV/nucleon ^{40}Ar+^{45}Sc collisions studied at midrapidity. Source radii are presented versus the transverse velocity for six different coalescence channels leading to charge one, two, and three fragments. Particular attention is paid to the temperature input in the model, as the extracted radii depend significantly on this parameter. A means of extracting the temperature from experimental data using the present model is described. Comparisons to the two temperature-dependent nucleon coalescence models will also be discussed.

I. INTRODUCTION

The measurement of the radius of the particle emission zone in heavy-ion collisions provides direct and fundamental information about the dynamical evolution of expanding systems of excited nuclear matter. This information allows estimates of the amount of collective expansion of the system before freeze-out, leading to the inference of densities. The comparison of source radii extracted for fragments of different masses can be used to infer the relative ordering of the freeze-out times of the different masses, and to infer the possible existence of liquid-gas or gas-plasma phase separation.

When significantly compressed and/or heated, nuclei expand and emit particles, some of which are composites formed by the fusion of some number of smaller particles inside the excited region. The energy-dependent probabilities for the particle emission and the radius of the region emitting these particles can be related by coalescence arguments [1,2]. These compare the invariant cross section for the formation of a particular composite of A nucleons to the momentum space density of nucleons raised to the Ath power. The result

is a dimensioned variable which, under specific assumptions, can be converted into the radius of the (expanding) source when two or more specific particles cease interacting by strong forces to form a specific composite. A density matrix coalescence formalism [3] which includes the consideration of the finite size of the composites has also been developed for the extraction of source radii. These concepts have previously been applied to study light fragment formation and source radii at LBL-Bevalac and BNL-AGS energies [2–10].

However, the extraction of source radii from coalescence phenomenology has been underutilized compared to two-particle correlation measurements for beam energies near and below ~100 MeV/nucleon. In this beam energy region, there are relatively large multiplicities of both nucleons and light fragments even in the most violent collisions. Fragment formation via the coalescence of two fragments must therefore be considered. Since the emission of light nuclei might be characterized by different source radii and lifetimes than for nucleon emission, the application of nucleon coalescence prescriptions is questionable in this case. For the formation of, e.g., ^{6}Li fragments, one can obtain more meaningful results by considering ^{3}H+^{3}He coalescence rather than the coalescence of six nucleons.

In this paper our goal is to clarify aspects of coalescence

*Electronic address: llope@physics.rice.edu

prescriptions, to show what additional insights a fragment coalescence analysis can provide, and to discuss the beam energies for which such an analysis is meaningful. The present model will then be used to extract results from recent experimental measurements of 55 and 115 MeV/nucleon ^{40}Ar+^{45}Sc collisions using the upgraded MSU 4π Array. The next section reviews the concepts of coalescence and reviews the previous nucleon coalescence prescriptions for the extraction of source radii. We present the fragment coalescence model in Sec. III, and the experimental results in Sec. IV. The implications of this analysis and the prospects for future measurements are discussed in Sec. V.

II. NUCLEON COALESCENCE MODELS

Nucleosynthesis via the coalescence of nucleons in heavy-ion collisions has been described in a variety of ways, and each approach allows the extraction of a source radius. In this section, these nucleon coalescence models are briefly reviewed to provide some perspective for the presentation of the fragment coalescence model, which is described in the next section. Generally, the variety of nucleon coalescence models can be grouped into four general categories: the empirical nucleon coalescence model [1,2], the thermodynamic nucleon coalescence model [2], the density matrix nucleon coalescence model [3], and the dynamic nucleon coalescence model [9,10].

The direct interaction, or final state, model of Butler and Pearson [11], which describes deuteron production, was extended to include triton, ^{3}He, and α-particle formation by Schwartzschild and Zupanic [12], as well as Gosset et al. [13]. These empirical nucleon coalescence models are based on the assumption that any two nucleons whose relative momentum is less than a certain value, p_0, coalesce to form a deuteron, while any three nucleons within this distance in momentum space form a triton, and so on. This model, however, implicitly assumes an infinite temperature. This makes this model unrealistic whenever the temperature of the particle emitting source is not significantly larger than the binding energy of the fragments assumed to be formed via coalescence. In particular, this is the case for the study of nucleosynthesis in heavy ion collisions at intermediate ener-

gies, i.e., at beam energies near and below ~ 100 MeV/nucleon, where the typical temperatures are less than ~ 10 MeV.

The empirical nucleon coalescence model was extended to allow for finite values of the temperature, and is called the thermodynamic (nucleon coalescence) model [2]. In this model, the invariant cross section for a particular composite, d^3N_A/d^3p_A, and the nucleon cross section, d^3N/d^3p, can be related to the volume, V, of the region within which the nucleons coalesce to form composites. Assuming that the composite is always formed in its ground state, this relationship reduces to

$$\frac{d^3N_A}{d^3p_A} = R_{np}^N A^3 \frac{2S+1}{2^A} \left(\frac{h^3}{V}\right)^{(A-1)} e^{B/T} \left(\frac{d^3N_N}{d^3p_N}\right)^A . \quad (1)$$

In this equation, h is Planck's constant, B, S, N, and A are the binding energy, spin, neutron number, and mass number of the composite, T is the temperature, and the factor $R_{np} = [(N_P+N_T)/(Z_P+Z_T)]$ is the ratio of neutron to proton numbers in the projectile and target nuclei. This model assumes that chemical and thermal equilibrium have been achieved, that the nucleons uniformly fill the collision volume, that the spatial proximity of the nucleons has no effect on probability for coalescence, and that the freeze-out occurs suddenly. In typical applications, it is furthermore assumed that the spectra of neutrons and protons are the same, so that the typically measurable proton cross section, d^3N_p/d^3p_p, can be used instead of d^3N_N/d^3p_N. This model does not consider the finite size of the fragment in its prediction of a source radius, which is given by $R = \sqrt{5/3}(3V/4\pi)^{1/3}$.

In the density matrix coalescence model of Sato and Yazaki [3] it is assumed that the emitted particles can be represented by density matrices. Finite values of the temperature can be included in the calculation. Chemical and thermal equilibrium are not assumed and the treatment is non-relativistic. Gaussian forms are assumed for the wave functions of the particles and the spatial distribution of these particles in the excited region within which the coalescence occurs. The size parameter, ν, of this region is given by solving

$$\frac{d^3N_A}{d^3p_A} = R_{np}^N A^{5/2} \frac{2S+1}{2^A} \left(\frac{\hbar}{m_0}\right)^{(A-1)} \left((1+\beta_T \nu_A) \frac{4\pi\nu_A \nu}{(\nu_A+\nu)}\right)^{(3/2)(A-1)} \left(\frac{d^3N}{d^3p}\right)^A , \quad (2)$$

where m_0 is the nucleon mass, and $\hbar = h/2\pi$. The quantity ν_A is the size parameter of the Gaussian wave function for the composite under consideration. The values of this parameter are $\nu_2 = 0.20$ fm^{-2} for deuterons, $\nu_3 = 0.36$ fm^{-2} for tritons and ^{3}He fragments, and $\nu_4 = 0.58$ fm^{-2} for alpha particles [14]. The temperature dependence is included in the quantity β_T, which is $\beta_T = \hbar^2/2m_0T$. This temperature dependence is not thermal, but rather results from the wave function overlap in the sudden approximation. If the fragments are created by interactions with third bodies, which have broad matrix elements, a thermal formalism is more

realistic [15]. The finite size of the fragment formed by coalescence is included in this model's prediction for the source radius, which is obtained from the equation, $R = \sqrt{5/2\nu}$.

Recently [9,10], coalescence prescriptions have been applied to event generating models that attempt to describe the dynamical evolution of the reaction. The dynamical calculation predicts the momenta and spatial positions of the all of the nucleons as a function of time. Two nucleons are assumed to fuse into a deuteron if their relative momentum, $\Delta p = |\vec{p}_1 - \vec{p}_2|$, and relative position, $\Delta R = |\vec{r}_1 - \vec{r}_2|$, are less than certain values appropriate for the known properties

of the deuteron. Relativistic effects can be included in the dynamical calculation if necessary, and any correlations between the position and momentum of nucleons, i.e., collective flow, as well as possible differences between the spectra of neutrons and protons, is implicit. The sudden approximation for the freeze-out is not assumed. These facts make dynamical nucleon coalescence calculations attractive for describing nucleosynthesis and source radii at LBL-Bevalac and BNL-AGS energies. However, such an approach is of questionable validity for intermediate energy collisions, where large-scale fluctuations are rampant due to liquid-gas phase separation. By focussing nucleons into relatively dense regions, the formation of fragments can be magnified. If the beam energy safely exceeds 100 MeV/nucleon, phase separation is less of an issue and such coalescence prescriptions become more realistic.

Dynamical descriptions of collisions in this energy range are provided by several different models. Boltzmann-Uehling-Uehlenbeck and other similar models consider only the evolution of the one-body phase space distribution, and hence do not include the fluctuations due to phase separation described above. Quantum molecular dynamics calculations do consider many-body correlations during the collision, and in principle predict the formation cross sections for all fragments, thus eliminating the need for coalescence models. However, since these models generally cannot reproduce the energy levels and degeneracies of light nuclei, it is not meaningful to make detailed comparisons of the predictions of these models with experimentally obtained fragment yields.

Less detailed comparisons that use the molecular dynamics code only to describe the initial stage of the reaction in a hybrid approach are less affected by such shortcomings; examples include Refs. [16] and [17].

III. FRAGMENT COALESCENCE MODEL

The previous coalescence prescriptions relate the spectra of, e.g., ^{6}Li fragments to the proton spectra raised to the sixth power, rather than through a binary fusion channel involving a ^{3}He and a triton. These methods would be equivalent if the nucleons and fragments are characterized by the same source radius and lifetime. Since this is generally not the case, a new model that considers the coalescence of light fragments into heavier ones is necessary. This model, called the fragment coalescence model, is presented in this section. It is a "progressive" coalescence prescription which allows the interpretation of the source radius for fragments of a given mass. For instance, by studying the channel ^{3}He$+$ $t \rightarrow ^6$Li, one can infer the source radius at that stage in the expansion when mass three fragments freeze-out.

Many previous phenomenological prescriptions were more complex than necessary, i.e., by introducing intermediate coalescence momenta. The Wigner approach is more transparent [15,18]. Also, since it is similar to standard interferometry formulas [19], it can readily be applied to Monte Carlo simulations. The formula governing the process in which two nucleons or fragments, labeled a and b, coalesce to form the composite, c, is

$$\frac{d^3N_c}{d^3p} = \mathscr{S} \int d^4x_a d^4x_b S_a\left(x_a, \frac{m_a}{m_a+m_b}(p_c)\right) S_b\left(x_b, \frac{m_b}{m_a+m_b}(p_c)\right) |\phi^2(x_a - v_c t_a - x_b + v_c t_b)|^2 \mathscr{B}(a,b,c;T), \qquad (3)$$

where ϕ is the relative wave function which is normalized such that it integrates to unity, and $S(x,p)$ is the probability of emitting a particle from space-time point x with momentum p. The spins of the particles combine to form the statistical factor $\mathscr{S}$, which is, $\mathscr{S} = (2S_c+1)/(2S_a+1)(2S_b+1)$. The Boltzmann factor, $\mathscr{B}(a,b,c;T)$, is

$$\mathscr{B}(a,b,c;T) = e^{(B_c - B_a - B_b)/T}, \qquad (4)$$

where T is the temperature, and B_i is the total binding energy of the fragment i.

By viewing the above formula in a frame where c is at rest, the terms proportional to v_c inside the argument of ϕ disappear, and the relativistic ambiguities are resolved. The inclusion of the Boltzmann term follows the assumption of local thermal equilibrium, where the particles are created at

the points x_a and x_b according to broad matrix elements and fill particular final states according to the available phase space.

By assuming Gaussian sources, Eq. (3) allows the extraction of the radius of the particle emitting system. We define the profile of the source using,

$$S(x,p) \propto \delta(t) e^{-r^2/2R_G^2}, \qquad (5)$$

where $\delta(t)$ is a delta function in the time, t. The wave function of the composite, ϕ, has the spatial extent, ρ_c, defined by

$$|\phi(\mathbf{r})|^2 \propto e^{-r^2/2\rho_c^2}. \qquad (6)$$

Then, the one-dimensional Gaussian radius is obtained by dividing the probabilities,

$$R_G^3 = \left(\frac{R_G^2}{R_G^2 + \rho_c^2/2}\right)^{3/2} \pi^{3/2} \frac{(2S_c+1)}{(2S_a+1)(2S_b+1)} \frac{(d^3N_a/d^3p_a)(d^3N_b/d^3p_b)}{d^3N_c/d^3p_c} \mathscr{B}(a,b,c;T). \qquad (7)$$

The size parameter of the composite's wave function, ρ_c, is given by [20] $\rho_c^2 = 1/2\nu_A$, where the parameter ν_A is that used as an input to the density matrix model described in the previous section, and A is the mass number of the composite c. We are unaware of a measurement of ν_A for fragments of mass six or greater. We have therefore used a polynomial extrapolation of the values of ν_2, ν_3, and ν_4 to obtain a value for ν_6, which resulted in $\nu_6 = 1.2 \text{ fm}^{-2}$. For the experimental data described in the next section, the first term in Eq. (7) is generally close to unity, so this extrapolation to a value of ν_6 is not expected to incur significant errors in the radius calculations for the mass six composites. The factor necessary to convert the one-dimensional Gaussian radius, R_G, given by Eq. (7), to the total radius assuming a spherical source, R, is given by

$$(4\pi)^{1/2}R_G = \left(\frac{4\pi}{3}\right)^{1/3} R, \qquad (8)$$

or, $R = 2.2R_G$.

The three cross sections (or invariant yields) are measured at the same velocity. For applications in which the particles are relativistic, the yields to be used in Eq. (7) are $(1/2\pi p_T)/(d^2N/dp_Tdy)$, where p_T and y are the transverse momentum and rapidity of the particles, respectively. The rapidity is defined by $y = \frac{1}{2}\ln[(E+P_Z)/(E-P_Z)]$, where E and P_Z are the total energy and the component of the momentum along the beam direction, respectively. For nonrelativistic particles, the one-dimensional Gaussian radius is obtained by solving

$$(R_G^2 + \rho_c^2/2)^{3/2} = \frac{(\hbar c)^3}{\beta^2\Delta\beta\Delta\Omega}\frac{\pi^{3/2}}{N_{ev}}\frac{(2S_c+1)}{(2S_a+1)(2S_b+1)}$$
$$\times \frac{M_c^3}{M_a^3M_b^3}\frac{N_aN_b}{N_c}\mathcal{B}(a,b,c;T). \qquad (9)$$

In this equation, the experimental multiplicities of the particles a, b, and c in a velocity bin of width, $\Delta\beta$, centered on the laboratory velocity, β, are given by N_a, N_b, and N_c. The masses of the three particles are M_a, M_b, and M_c. The solid angle subtended by the detector measuring a, b, and c is $\Delta\Omega$, and the number of events included in the analysis is given by N_{ev}.

The justification for the present fragment coalescence model is different for the coalescence of heavier particles than it is for, e.g., the $p+p\rightarrow d$ channel. For proton coalescence, one can derive Eq. (3) by assuming that the two protons scattered with broad randomizing matrix elements. For the coalescence of heavier fragments, such as in the $t+{}^3$He $\rightarrow {}^6$Li channel, one must justify the fact that all six nucleons have been able to move into the same region of phase space. Thus the present fragment coalescence formalism requires the assumption of local chemical equilibrium.

The prescription is of dubious applicability for beam energies where there is strong liquid-gas or gas-plasma coexistence. Coalescence implies an exponential mass spectrum, but, for intermediate energy collisions, many fragments could come from the dissolution of the liquid phase, which leads to a much broader mass spectrum. Fragments can also be emitted in the decays of heavier fragments. These "addi-tional" sources of fragments significantly suppress the radii obtained from such models. Even at rather high beam energies, such a component could exist in the spectator momentum regions. Thus, while deuteron coalescence should be valid even at low energies, lithium coalescence becomes valid only for beam energies above $\sim$50 MeV/nucleon, and then only in the participant region.

These qualifications are not much different than the caveats that accompany two-particle correlation phenomenology. For instance, when interpreting $\pi+\pi$ interferometry in highly relativistic collisions, one must be careful to account for the effects of long-lived resonances. In this energy regime, interferometry can also be affected by clustering, in analogy to the fragments coming from the liquid phase in intermediate energy collisions. In such a situation, anomalously small sizes from $p+p$ and K^++K^- correlations can be used as a signal for gas-plasma phase separation [21]. The same statement could be made here. If the source sizes from heavier coalescence combinations are significantly smaller than those for lighter coalescence channels, this could be interpreted as a signal that fragments are emitted from a smaller fraction of the overall source volume due to phase separation.

Radii extracted from coalescence models and two particle interferometry can also be affected if there is a significant amount of collective flow in the excited system, or if the system is relatively long lived. If there is flow, the emission points of two particles of a specific velocity are concentrated into specific regions of the expanding emission volume. Depending on the magnitude of the flow, this may magnify the fragment formation and suppress the apparent radius, in similarity to the effects of phase separation. An opposite effect is caused by long-lived sources, which lead to final states containing many evaporated particles. Due to the Coulomb and angular momentum barriers, primarily light particles are emitted by evaporation and the apparent source radius is enhanced.

It is important to assess the importance of the flow and long lifetime effects for the data described in the next section. The magnitude of the transverse flow in the present sample of events is expected to be smaller than that reported in Ref. [22] given the more central event selection chosen for this work. We estimate that the transverse flow as defined in Ref. [22] is less than $\sim$10 MeV in the present events. A recent analysis [23] of central ^{36}Ar+^{27}Al collisions at a beam energy of 55 MeV/nucleon found that the radial flow was $\sim$0.5 MeV/nucleon. At the highest energy, a unique value of the radial flow was not seen for all particles, but values of $\sim$2 MeV/nucleon were obtained for the nucleons and light fragments. These transverse and radial flow values should be contrasted with the excitation energies in the present events [17], which are about an order of magnitude larger. The boundary in beam energy between evaporative and explosive emission time scales is $\sim$45–55 MeV/nucleon for central ^{84}Kr+^{93}Nb reactions [31]. The systematics of Ref. [24] imply a value near this, if not slightly larger, for central ^{40}Ar+^{45}Sc reactions. A lifetime of 30 fm/c was found [25] for central ^{36}Ar+^{45}Sc reactions at 80 MeV/nucleon. Therefore, effects on the extracted radii due to the

lifetime of the source are negligible for the present 115 MeV/nucleon data, but are not necessarily negligible for the 55 MeV/nucleon data.

The temperature is a particularly important input parameter for all three of the models discussed above. In these models, the extracted radii decrease rather strongly with increases in the value of the temperature assumed in the calculation (see the following section). One is therefore motivated to make an experimental measurement of this quantity.

One method for measuring the temperature involves the two particle correlations of a pair of particles, such as $d + \alpha$, that would be emitted in the decay of fragments with low lying excited states [26,27]. Another method involves the definition of a temperature scale based on ratios of the yields of ^{3}He, α, ^{6}Li, and ^{7}Li fragments [28]. A temperature can also be extracted from the present model. In the formalism outlined above, the $p + t \rightarrow \alpha$ channel could be replaced by the $d + d \rightarrow \alpha$ channel, allowing one to extract the source radius for fragment coalescence into α particles in two different ways. If one assumes that these two channels are characterized by the same actual radius, the temperature of this source can by extracted by requiring that these two channels result in the same apparent radius.

IV. EXPERIMENTAL RESULTS

In this section, we present experimental results obtained from the fragment coalescence model for six different channels leading to charge one, two, and three fragments. We will compare the results from the present model to those obtained from the thermodynamic nucleon coalescence model and density matrix nucleon coalescence model. As the three prescriptions depend significantly on the temperature input, estimates of the temperatures appropriate for the data must be attempted. The data discussed below consists of 55 and 115 MeV/nucleon ^{40}Ar+^{45}Sc reactions that were measured with the recently upgraded MSU 4π Array, using beams from the K1200 Cyclotron at the National Superconducting Cyclotron Laboratory.

The upgraded MSU 4π Array consists of several newly installed close-packed forward arrays, and a main ball of phoswich detectors fronted by Bragg Curve Counters (BCC's) run in ion chamber mode. The main part of the new forward arrays, called the High Rate Array (HRA) [22], consists of 45 phoswich detectors that cover the laboratory polar angles from $\sim 3°$ to $\sim 18°$. The HRA sub-elements subtend solid angles that range from 5.1 to 6.9 msr, and provide better than half a unit of charge resolution for charges from $Z = 1$ to that of the ^{40}Ar projectile. Isotopic resolution was obtained for charge one fragments. The main ball covers the polar angles from $\sim 18°$ to $\sim 162°$, with thirty hexagonal and pentagonal detector modules arranged in a truncated icosahedron, or soccer-ball, geometry. Each hexagonal(pentagonal) module is subdivided into six(five) distinct detector subelements which subtend 64.5 (48.5) msr. The 170 phoswich detectors of the main ball resolve charges from $Z = 1$ to ~ 8, and isotopically resolve charge one particles. The BCC's resolve charges from $Z = 3$ to $Z \sim 18$. The velocity thresholds for the main ball (HRA) detectors are $\sim 5(4.5)$ cm/ns for protons, $\sim 4(4.5)$ cm/ns for deuterons and tritons, $\sim 4.5(4)$ cm/ns for heliums, and $\sim 5(4.5)$ cm/ns for lithiums.

One must restrict coalescence analyses to kinematic regions for which particle emission from projectile and targetlike sources is negligible. In this analysis, the contribution to the particle multiplicities from spectator source emission is suppressed in two ways. First, a strict selection of central collisions is made. This involves a two-dimensional cut on the total charged particle multiplicity and the total transverse kinetic energy, which selects approximately 5% of the minimum bias events. This corresponds to average impact parameters of $\sim 0.22 b_{max}$, where b_{max} is the largest impact parameter which satisfies the trigger condition used during the data collection (two charged particle hits in the main ball). According to Ref. [22], the comparison of the events from this trigger to those from a less selective trigger (one charged particle hit in the HRA) implies that $b_{max} \sim (0.88 \pm 0.04)[R_P + R_T]$. For the presently considered small impact parameters, the excellent coverage (-0.6ex$\leq$94%) of the upgraded MSU 4π Array still allows the measurement of particles arising from projectile and targetlike sources. We therefore restrict the analysis to those particles emitted at midrapidity. This selection involves the cut $-0.2 < y^{c.m.}/y_{proj}^{c.m.} < 0.2$, where $y^{c.m.}(y_{proj}^{c.m.})$ is the rapidity of the particle (projectile) measured in the projectile-target center of momentum frame.

Since the ^{40}Ar+^{45}Sc system has little neutron excess and the 55 and 115 MeV/nucleon beam energies studied below lead to excitation energies that are well above the Coulomb barrier [17], we assume that the neutron and proton spectra are equivalent, as well as the triton and ^{3}He spectra. We also assume that the temperature is a known quantity, although an method for extracting the appropriate temperature for these data using the present model is discussed below.

In these data, the helium and lithium isotopes are not resolved. Below, we present a method for artificially separating the measured multiplicities of $Z = 2$ and $Z = 3$ fragments into the multiplicities of the various helium and lithium isotopes. Disentangling the isotopic composition as discussed below is rather crude, especially since the model presented in the previous section requires the comparison of spectra at the same velocity. Without the experimental resolution of the helium and lithium isotopes, the isotope velocities are computed assuming the most common isotope. This introduces additional errors on the order of $\sim 15\%$ for any channel involving ^{3}He and heavier fragments. These systematic errors are added in quadrature to the statistical errors for all of the results discussed below. We stress that the present model is considerably more powerful if applied to experimental data including the isotopic resolution of all light fragments.

By writing Eq. (7) for the reactions $p + t \rightarrow \alpha$, $p + d \rightarrow {}^3$He, and $t + t \rightarrow {}^6$He, one is left with three equations and four unknowns: $R_G, dN_{^3\text{He}}/d^3v$, dN_α/d^3v, and $dN_{^6\text{He}}/d^3v$. The sum of the three helium yields is experimentally measured, which supplies the fourth condition. This allows the extraction of R_G in $Z = 2$ isotopically unresolved data under the assumption that the channels $p + t \rightarrow \alpha$, $p + d \rightarrow {}^3$He, and $t + t \rightarrow {}^6$He are characterized by the same source radius. The channel $p + t \rightarrow \alpha$ can be replaced with the channel $d + d \rightarrow \alpha$, yielding a second determination of the source radius. By requiring that these two channels yield the
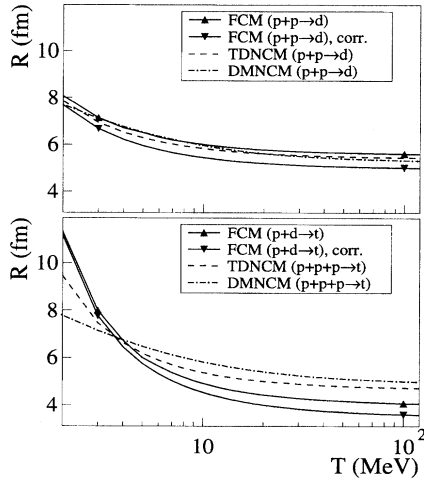
FIG. 1. The source radii from the present fragment coalescence model (FCM) without the correction for the finite size of the fragments (solid lines, up triangles), with this correction (solid lines, down triangles), from the thermodynamic nucleon coalescence model (TDNCM), and from the density matrix nucleon coalescence model (DMNCM), versus the temperature for the central 115 MeV/nucleon ^{40}Ar+^{45}Sc reactions viewed at midrapidity. The upper (lower) frame depicts the results for deuteron (triton) coalescence.
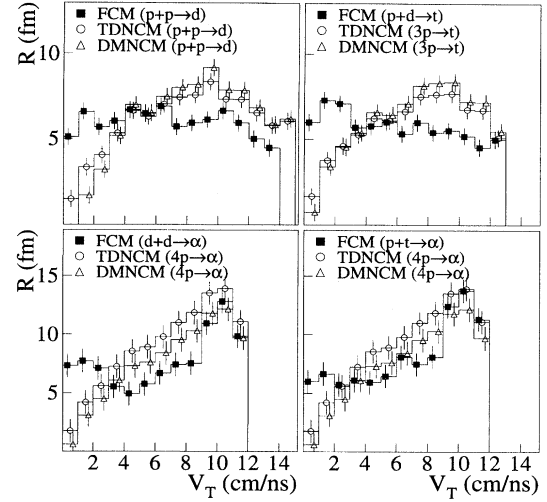

FIG. 2. The source radii versus the transverse velocity obtained from the present FCM are compared to those from the TDNCM and the DMNCM for the central 115 MeV/nucleon ^{40}Ar+^{45}Sc reactions viewed at midrapidity. A temperature of 5 MeV was assumed, and the correction for the finite size of the fragments was included in the FCM calculations.

same radius, one can determine an appropriate temperature, and its dependence on the particle velocity. This is discussed later in the paper.

This exercise can be repeated for the coalescence of Li fragments in the channels $d+\alpha \rightarrow {}^6$Li, $t+\alpha \rightarrow {}^7$Li, ^{6}He+d $\rightarrow {}^8$Li, and $t+{}^6$He$\rightarrow {}^9$Li. In these cases, the yields for the various helium isotopes come from the calculation described in the previous paragraph. In the calculations of source radii, we opt in general for the more symmetric channels of those that are available. For example, we choose to use the $t+\alpha \rightarrow {}^7$Li channel rather than the $p+{}^6$He$\rightarrow {}^7$Li channel, since it is likely that protons and ^{6}He fragments are characterized by different source radii and lifetimes.

The comparison of the source radii extracted from the fragment coalescence model (FCM) are compared to those obtained from the thermodynamic nucleon coalescence model (TDNCM) and the density matrix nucleon coalescence model (DMNCM) is shown versus the temperature in Fig. 1 for the central 115 MeV/nucleon ^{40}Ar+^{45}Sc reactions. The upper (lower) frame depicts the predictions for deuteron (triton) coalescence. The solid lines with the down triangles (down triangles) depict the FCM results with (without) the correction for the finite size of the fragments. This correction is ignored by simply setting $\rho_c=0$ in Eq. (9). The entire range of temperatures shown in this figure should not be taken as realistic for this reaction. The horizontal axis is extended far beyond a more plausible range of temperatures only to indicate the limiting values of the radii for arbitrarily large temperatures. In this figure, the results for all three models are an unweighted average over the velocity of the fragments.

For deuteron coalescence, the results from the uncorrected FCM are within ~ 0.4 fm of the TDNCM and DMNCM predictions for all of the temperatures shown in this figure.

The correction to the FCM results for the finite size of the fragments reduces the extracted radii by ~ 0.5 fm. For the triton coalescence, the FCM results are larger (smaller) that the predictions from the other two models for temperatures that are smaller (larger) than ~ 4 MeV. It is important to note that the TDNCM does not consider the finite size of the composite, while the FCM and DMNCM do. It is therefore surprising that the predictions from the DMNCM are generally significantly different from those obtained from the FCM. An important difference between the TDNCM and DMNCM models as compared to the FCM is that the binding energy of the deuteron is included in the Boltzmann term used in the FCM.

The dependence of the source radius on the transverse velocity, defined as $V_T = V \sin(\theta)$ where V is the composite's velocity and θ is its polar angle, is shown in Fig. 2 for deuteron, triton, and α-particle coalescence obtained from the three models. A temperature of 5 MeV was assumed. The results for α-particle coalescence, shown in the lower two frames of this figure, change by less than ~ 0.4 fm if the multiplicities used in the calculations are taken from the deconvolution described above, or simply taken from as the experimentally measured multiplicity of $Z=2$ fragments.

For the deuteron and triton channels and a temperature of 5 MeV, shown in the two upper frames, the FCM-extracted radii are near ~ 6.5 fm, and are only weakly dependent on the transverse velocity. The TDNCM and DMNCM predictions are similar for each channel, and depend more significantly on the transverse velocity. The radii obtained from these two models are smaller (larger) than those obtained from the FCM for transverse velocities smaller (larger) than roughly 6 cm/ns. The radii extracted for the two α-particle FCM channels, $d+d \rightarrow \alpha$ and $p+t \rightarrow \alpha$, are on the order of 6 fm for transverse velocities below ~ 9 cm/ns, and are significantly larger for larger transverse velocities. The TDNCM

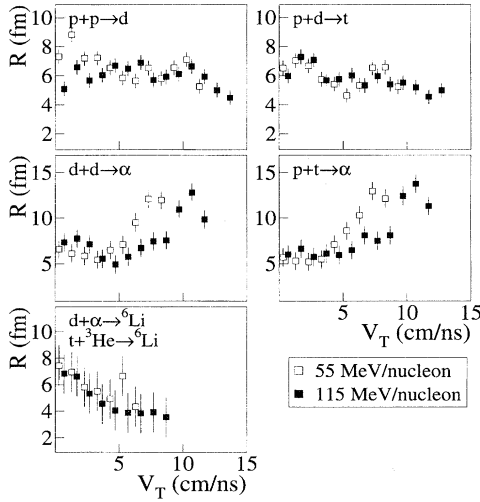FIG. 3. The source radii extracted from six different FCM channels versus the transverse velocity for the central 115 MeV/nucleon ^{40}Ar+^{45}Sc reactions viewed at midrapidity. A temperature of 5 MeV/nucleon was assumed, and the correction for the finite size of the fragments was included.
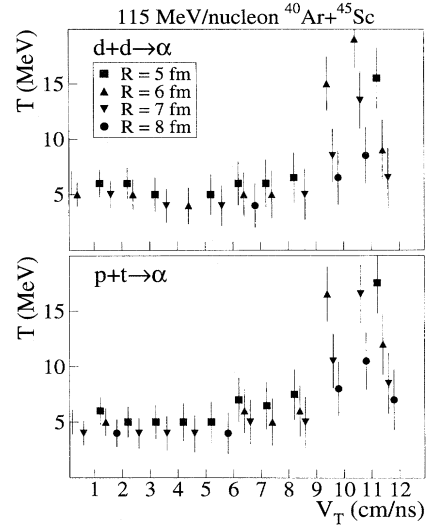
FIG. 4. The temperature leading to radii of 5 (squares), 6 (up triangles), 7 (down triangles), and 8 (circles) fm versus the transverse velocity for the two FCM channels leading to α particles in the central 115 MeV/nucleon ^{40}Ar+^{45}Sc reactions studied at mid rapidity. The finite size correction was included in the calculation.

and DMNCM results show a similar, but smoother, dependence on the transverse velocity. In similarity to the results for the deuteron and triton channels, the TDNCM and DMNCM predictions for the α-particle channels are significantly smaller than those from the FCM for low transverse velocities.

Figure 3 depicts the source radii from the FCM for six different channels leading to charge one (upper frames), two (middle frames), and three (lower frame) fragments versus the transverse velocity. The results for the 55 (115) MeV/nucleon ^{40}Ar+^{45}Sc reaction are shown as the open (solid) squares, and a temperature of 5 MeV was assumed. The source radii extracted from two proton interferometry of ^{36}Ar+^{45}Sc collisions at 80, 120, and 160 MeV were $\sim$7–8 fm [25,29]. This radius is somewhat larger than that extracted from the $p+p\rightarrow d$ channel in our 115 MeV/nucleon data using the FCM and a temperature of 5 MeV. The present FCM radii agree with that presented in Refs. [25] and [29] if a temperature of $\sim$4 MeV is used in the model.

Using the fireball model [30], the impact parameter region studied herein corresponds to $\sim$70 participant nucleons. Dividing this number by the volume $4\pi R^3/3$ gives a breakup density of about forty percent of normal nuclear matter density when using R=6.5 fm. The true freeze-out density would be somewhat smaller than this value if the actual temperature is smaller than 5 MeV. Also, the overall radius may increase slightly upon consideration of the effects of collective flow.

The effective source radii for both the 55 and 115 MeV/nucleon data decrease as one considers coalescence into increasingly heavier fragments. This may be due to the (relatively weak) collective expansion of the matter which concentrates heavier particles of a given velocity in a smaller region of the source. Alternatively, it may result from phase separation, which would focus fragments into the smaller regions of the source with high densities. By combining coa-

lescence analyses with nucleon-nucleon and Coulomb-induced two fragment interferometry, one can determine the cause of this behavior. Qualitatively, this behavior was observed at the Bevalac [4], but in this analysis the Boltzmann factor was not included and the centrality of the events was not well characterized.

The apparent source sizes vary little for the two beam energies, which agrees with the behavior seen using two nucleon interferometry [25,29], as well as two fragment correlations which are governed by Coulomb repulsion [31–33]. The radii from the central 55 MeV/nucleon reactions are generally larger that those from the 115 MeV/nucleon reactions for α coalescence. According to the discussion in the previous section, this would imply an α source lifetime for the 55 MeV/nucleon reactions that is significantly larger than that for the 115 MeV/nucleon reactions.

In the two α-particle channels, the FCM indicates a significant increase in the apparent source size at the largest transverse velocities when a constant temperature of 5 MeV is assumed (cf. Figs. 2 and 3). We present an alternative view in Fig. 4. In this figure, the temperatures that lead to specific source radii equalling 5, 6, 7, and 8 fm are shown versus the transverse velocity for these two FCM channels. For small transverse velocities, these source radii are realized over a relatively small temperature interval near $\sim$5 MeV. However, for the large transverse velocities, temperatures significantly higher than 5 MeV lead to FCM radii similar to those measured at the low transverse velocities. The relatively large radii shown in Figs. 2 and 3 for helium and lithium coalescence at large values of the transverse velocity can therefore occur if the temperatures corresponding to these velocities are significantly larger than 5 MeV.

Such an observation clearly underscores the need of an independent measurement of the temperature versus the transverse velocity. Temperature measurements have previ-
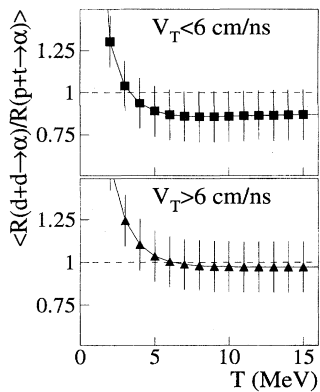
FIG. 5. The ratio of the $d+d\rightarrow\alpha$ and $p+t\rightarrow\alpha$ source radii extracted from the present FCM versus the temperature used in the calculation for transverse velocities $V_T<6(V_T>6)$ cm/ns in the central 115 MeV/nucleon ^{40}Ar$+^{45}$Sc reactions at midrapidity. The finite size correction was included.

ously been performed in two different ways (see Refs. [26–28]). A temperature can also be extracted from the present model by requiring that the source radius from, e.g., the FCM channel $d+d\rightarrow\alpha$ equals that from the $p+t\rightarrow\alpha$ channel, under the assumption that these two channels are characterized by the same source radius and lifetime. The temperatures extracted in this way for the present data will necessarily contain the uncertainty resulting from the lack of isotope resolution for the charge two fragments.

Nonetheless, as an example of the extraction of the temperature using the FCM, we plot the ratio of the radii extracted from the $d+d\rightarrow\alpha$ and $p+t\rightarrow\alpha$ channels versus the temperature used in the calculation in Fig. 5. The upper (lower) frame depicts this ratio for transverse velocities smaller (larger) than 6 cm/ns. By assumption, the correct temperature results in a value of unity for this ratio. The uncertainties in this ratio resulting from the lack of isotope resolution for the helium fragments is added in quadrature to the statistical uncertainties and depicted as the error bars. It is inferred that the temperature is larger than ∼2 MeV for the lower transverse velocities, and larger than ∼4 MeV for the larger transverse velocities. Values of unity for this ratio occur at ∼4 (6) MeV for $V_T<(>)6$ cm/ns. This supports the interpretation of Fig. 4 that was discussed above. The larger transverse velocity fragments are emitted at significantly larger temperatures than those appropriate for the lower velocity fragments. This implies that the fragments with large transverse velocities are emitted at an early stage in the reaction, when the temperatures are significantly higher than they are when the fragments with smaller transverse velocities are emitted.

V. CONCLUSIONS

A new model, called the fragment coalescence model, was presented which considers nucleosynthesis by the coalescence of fragments rather than nucleons. The model can in principle be applied to reactions at any beam energy. It is, however, particularly suitable for intermediate energy reactions, where comparable multiplicities of both nucleons and light fragments result from central collisions. The informa-

tion that is obtained from this model is complementary to that obtained with two proton [25,34] and two deuteron [35] correlations, as well as Coulomb-induced correlations of heavier fragments such as two carbons [31–33]. It is complementary also to the few correlation measurements using two light fragments [26,36] such as $d+\alpha$. Like other temperature-dependent nucleon coalescence models, this model allows the extraction of source sizes for fragments of a specific mass and velocity. If the nucleons and light fragments would be characterized by the same source radius and lifetime, the present model predicts source radii that are similar to those obtained from the previous models. In general however, this is not the case, and the present model gives more realistic predictions for the source radii via the coalescence of fragments as compared to those from nucleon coalescence prescriptions. Under the assumption that a given pair of fragment coalescence channels are characterized by the same source, the temperature of this source can also be extracted from the present model, and as a function of the fragment velocity.

The advantages of this coalescence model for the extraction of source radii are several as compared to interferometric measurements. First, one does not need to make time consuming high-statistics coincidence measurements in small relative momentum bins. Hence, it can be applied to data taken with a single detector, assuming that the impact parameter is suitably constrained and that the particle emission from spectator sources is sufficiently suppressed. One does not need high momentum resolution as is the case for most interferometric measurements, which makes the analysis applicable to data taken with devices with somewhat poorer resolution but better kinematic coverage. However, the potential of analyses involving the present model will not be fully exploited until the experimental measurements are made with isotopic resolution for all of the light fragments. One would then have a wide variety of fragment combinations to study, which, when combined with this model's ability to obtain the effective local temperature as a function of the fragments' velocity, would give valuable insights into the dynamics of the reaction.

This present model was applied to experimental data on central 55 and 115 MeV/nucleon ^{40}Ar$+^{45}$Sc reactions studied at midrapidity with the recently upgraded MSU 4π Array. Most of the qualitative and quantitative results of this analysis were consistent with expectations. The source sizes extracted from our analysis are the similar to those obtained from previous interferometric measurements of ^{36}Ar$+^{45}$Sc reactions, and imply approximate freeze-out densities of about forty percent of normal nuclear matter density. The apparent source sizes for increasingly heavier fragments decreased, consistent with either collective expansion or liquid-gas phase separation. The comparison of the radii from the 55 and 115 MeV/nucleon reactions in the heavier coalescence channels implies the importance of source lifetime effects in the lower energy data.

The surprising result of the present analysis is in the behavior of the source radii as a function of the fragments' transverse velocity. The general expectation is that the apparent source radii decrease with increasing transverse velocities due to both collective expansion and cooling effects. The

deuteron and triton FCM radii exhibit such a trend. However, for helium and lithium coalescence and a fixed temperature input to the FCM, the apparent radii are largest at the largest transverse velocities. We showed that this behavior can result from a relationship between the local source temperature and the transverse velocity. Experimental data including isotopic resolution for all of the light fragments should be studied using the FCM to quantify this observation.

[1] A.Z. Mekjian, Phys. Rev. Lett. **38**, 640 (1977); Phys. Rev. C **17**, 1051 (1978); Nucl. Phys. **A312**, 491 (1978).

[2] S. Das Gupta and A.Z. Mekjian, Phys. Rep. **72**, 131 (1981).

[3] H. Sato and K. Yazaki, Phys. Lett. **98B**, 153 (1981).

[4] B.V. Jacak, D. Fox, and G.D. Westfall, Phys. Rev. C **31**, 704 (1985); B.V. Jacak *et al.*, *ibid.* **35**, 1751 (1987).

[5] H. Gutbrod, A. Sandoval, P. Johansen, A. Poskanzer, J. Gosset, W. Meyer, G. Westfall, and R. Stock, Phys. Rev. Lett. **37**, 667 (1981).

[6] M.C. Lemaire, S. Nagamiya, S. Schnetzer, H. Steiner, and I. Tanihata, Phys. Lett. **85B**, 38 (1979).

[7] G. Kunde *et al.*, Phys. Rev. Lett. **74**, 38 (1995).

[8] A.J. Baltz, C.B. Dover, S.H. Kahana, Y. Pang, T.J. Schlagel, and E. Schnederman, Phys. Lett. B **325**, 7 (1994).

[9] J. Nagle, B.S. Kumar, M.J. Bennett, G.E. Diebold, J.K. Pope, H. Sorge, and J.P. Sullivan, Phys. Rev. Lett. **73**, 1219 (1994); J. Nagle, B.S. Kumar, M.J. Bennett, S.D. Coe, G.E. Diebold, J.K. Pope, A. Jahns, and H. Sorge, *ibid.* **73**, 2417 (1994).

[10] J. Barrette *et al.*, Phys. Rev. C **50**, 1077 (1994).

[11] S.T. Butler and C.A. Pearson, Phys. Rev. **129**, 836 (1963).

[12] A. Schwartzschild and Ć. Zupanic, Phys. Rev. **129**, 854 (1963).

[13] J. Gosset *et al.*, Phys. Rev. C **16**, 629 (1977).

[14] J.C. Bergstrom, Nucl. Phys. **A327**, 458 (1979).

[15] S. Pratt, Phys. Rev. C **40**, 168 (1989).

[16] M.B. Tsang *et al.*, Phys. Rev. Lett. **71**, 1502 (1993).

[17] W.J. Llope *et al.*, Phys. Rev. C **51**, 1325 (1995).

[18] M. Gyulassy, K. Frenkel, and E.A. Remler, Nucl. Phys. **A402**, 596 (1983).

[19] W. Bauer, C.K. Gelbke, and S. Pratt, Annu. Rev. Nucl. Part. Sci. **42**, 77 (1992).

[20] In Ref. [3], the wave function of the composite is defined as $\phi(\mathbf{r}) \propto \exp(-\nu r^2)$, whereas Eq. (6) is used herein.

[21] S. Pratt, Phys. Rev. C **49**, 2722 (1994).

[22] R. Pak *et al.*, Phys. Rev. Lett. (submitted).

[23] J.C. Steckmeyer *et al.*, Proceedings of the XXXIII International Winter Meeting on Nuclear Physics, Bormio, Italy, 1995 (LPC CAEN Report No. LPCC 95-04) (unpublished).

[24] W.J. Llope *et al.*, this issue, Phys. Rev. C **52**, 1900 (1995).

[25] M.A. Lisa *et al.*, Phys. Rev. Lett. **71**, 2863 (1993).

[26] T.K. Nayak *et al.*, Phys. Rev. C **45**, 132 (1992).

[27] C. Schwarz *et al.*, Phys. Rev. C **35**, 376 (1993).

[28] J. Pochodzalla *et al.*, Phys. Rev. Lett. **75**, 1040 (1995).

[29] D. Handzy *et al.*, "Understanding Proton Emission in Central Heavy-Ion Collisions," MSU Report (1995).

[30] G.D. Westfall *et al.*, Phys. Rev. Lett. **37**, 1202 (1977); J. Gosset *et al.*, Phys. Rev. C **16**, 629 (1977).

[31] E. Bauge *et al.*, Phys. Rev. Lett. **70**, 3534 (1993).

[32] T. Glasmacher *et al.*, Phys. Rev. C **50**, 952 (1994).

[33] D. Fox *et al.*, Phys. Rev. C **50**, 2424 (1994).

[34] N. Xu *et al.*, Nucl. Phys. **A566**, 585c (1994).

[35] W. Gong *et al.*, Phys. Rev. C **47**, R429 (1993).

[36] J. Pochodzalla *et al.*, Phys. Lett. B **174**, 36 (1986); Phys. Rev. C **35**, 1695 (1987).